Journal of the European Ceramic Society 16 (1996) 339–351

0955-2219/96/$15.00
0955-2219(95)00174-3

Transmission Electron Microscopy of Microstructures in Ceramic Materials

Hans-Joachim Kleebe,[a] Wolfgang Braue,[b] Hans Schmidt,[a] Giuseppe Pezzotti[c] & Günter Ziegler[a]

[a]University of Bayreuth, Institute of Materials Research, Ludwig-Thoma-Str. 36B, D-95447 Bayreuth, Germany
[b]German Aerospace Research Establishment (DLR), Materials Research Institute, Linder Höhe, D-51147 Cologne, Germany
[c]Toyohashi University of Technology, Department of Materials Science, Hibarigaoka, Tempaku-cho 1-1, Toyohashi 441, Japan

(Received 4 July 1995; accepted 10 September 1995)

Abstract

Based on selected examples from the area of Si_3N_4 ceramics, the value of utilizing transmission electron microscopy (TEM) as a technique to study ceramic microstructures as well as a characterization tool for the development of new materials is demonstrated. In the field of 'new ceramics', one Si_3N_4-based composite is discussed, which was processed via pyrolysis of liquid precursors (polysilazanes). Moreover, it is shown that TEM in general can helpfully accompany ceramic processing techniques. This applies to the characterization of ceramic starting powders as well as to the study of densified materials. The investigation of Si_3N_4 powders, in particular the influence of the addition of sintering aids via organometallic precursors, which leads to a homogeneous distribution of sintering additives in the powder compact, in contrast to the use of metal oxide powders, is shown. The variation of microstructures during the densification process of liquid assisted sintering is also demonstrated. The most common application of the TEM technique is to characterize dense ceramic components in the as-processed (as-sintered) state. Post-sintering heat treatment can initiate secondary phase crystallization. However, the very important aspect of microstructure integrity at elevated temperatures, e.g. the stability of microstructures under severe service conditions, is also addressed. Emphasis is placed on the fact that ceramic microstructures, which are typically thought to be rather stable, can undergo serious microstructural changes when temperature and stress is applied simultaneously, which strongly limits potential applications of these materials.

1 Introduction

It is well established that transmission electron microscopy (TEM) is a very helpful and powerful technique to characterize microstructures of materials in detail. It is way beyond the scope of this paper to review all major contributions in materials science which are related to TEM, however, it should be emphasized that this technique allows the gathering of a wide variety of different information with respect to microstructure and/or composition with high spatial resolution.[1,2] The main areas of information covered by TEM investigations are: (i) conventional imaging; (ii) electron diffraction; (iii) chemical microanalysis–EDX, EELS; (iv) high-resolution imaging and (v) magnetic structure imaging–Lorentz microscopy. Apart from diffractional data, obtained by either selected area (SAD) or convergent beam electron diffraction (CBED) techniques,[3,4] which allow phase identification as well as space group determination or residual stress analysis, one of the major contributions of TEM to materials science is the enlarged understanding of materials performance.[5–8] This is based on the correlation between microstructural features observed during TEM inspection and bulk material properties. In order to tailor materials to meet specific requirements such as high temperature performance, the relationship between processing, microstructure, and mechanical behaviour has to be known. Therefore, this paper intends to underline the importance of TEM analysis to materials science in general and, in particular, to the processing and development of ceramics. However, it should be emphasized that the information obtained by TEM with respect to the overall ceramic microstructure is the final result of a number of processing steps involved, each of which plays an important role during microstructure development.[9,10] Hence, materials characterization can be rationalized in terms of: (i) powder processing; (ii) powder compacts; (iii) development during

sintering — temperature and time dependence; (iv) as-sintered microstructure and (v) variation of microstructure under service conditions.

The studies reported here focus on Si_3N_4-based ceramics as one representative of the important materials group of structural ceramics for technical and engineering applications. Emphasis is placed on the fact that TEM is a favourable technique to characterize the materials along the different processing steps involved in the production of dense components. In addition to the microstructural development of Si_3N_4-based materials, processed via the two major processing routes utilized today, i.e. powder processing and organometallic precursors, the variation of microstructure under service conditions, as observed by TEM, is also discussed. Hence, processing of Si_3N_4 ceramics is characterized from its origin, the powder particle and doping of starting powders with sintering aids, through the formation of a dense body to the performance of the final product at elevated temperatures and higher local stresses. It should be noted here that the observed degradation in microstructure stability under testing conditions seemingly suggests a rather limited potential of Si_3N_4 ceramics for high-temperature performance.

2 Experimental Procedures

2.1 Materials preparation

Processing of different silicon nitride-based ceramics was accompanied by transmission electron microscopy studies, in order to characterize microstructural development during subsequent processing steps. Incorporation of sintering additives was made by both mixing/milling of the Si_3N_4 powders with the metal oxide, (e.g. Y_2O_3, HC-Starck) and by utilizing soluble organometallic compounds (Y-ethanolate, Aldrich) which react with the surface silanol groups in a non-aqueous solvent. In case of organometallic doping, the corresponding metal oxide is formed after calcination at an elevated temperature of approximately 800°C. The respective processing steps involved to form dense sintered (SSN) or dense post-sintered reaction bonded Si_3N_4 materials (SRBSN) via gas-pressure sintering (GPS) are reported in detail elsewhere.[11] GPS usually follows four distinct dT/dt ramps. The increase from RT to 1100°C was achieved in about 1 h, followed by two 30 min intervals for the ramps between 1100 and 1300°C and between 1300 and 1875°C. To ensure the formation of closed porosity within the presintered body, the experiment was held for 20 min at 1875°C (p_{N_2} = 1·5 MPa). Thereafter, the N_2-pressure was increased to 10 MPa with the temperature raised to 1925°C and held for 60 min. During gas-pressure sintering, a dilatometer was attached to the specimen surface in order to register both linear shrinkage and densification rate during sintering.

Processing of Si_3N_4-based ceramics via organometallic precursors was performed by the synthesis of polycarbosilazanes at room temperature by the ammonolysis of substituted chlorosilanes R_ZSiCl_{4-z} (R = H, alkyl, CH = CH_2). The reaction which is given in (1) was

$$n\ R_ZSiCl_{4-z} + NH_3(\text{excess}) \Rightarrow [R_ZSi(NH)_{(4-z)/2}]n + n(4-z)\ NH_4Cl \quad (1)$$

carried out in dry toluene.[12] After removing both ammonium chloride and solvent the remaining liquid polysilazanes yields 75–85%. Purity and structure of the precursors were determined spectroscopically and by chemical analysis.[13] Precursor synthesis, processing and characterization were performed in an inert gas atmosphere (Schlenk technique, glove box) to avoid the incorporation of oxygen. Crystallization as well as reaction behaviour of the materials were investigated at temperatures up to 1600°C.*

2.2 Microstructure characterization, TEM studies

The overall microstructural characterization of the Si_3N_4 materials investigated was performed by transmission electron microscopy (TEM) utilizing a Philips CM20FEG (field emission gun) microscope fitted with both an ultra-thin window Ge energy dispersed X-ray (EDX) detector and a PEELS spectrometer. Operating at 200 kV, the instrument reveals a point resolution of 0·24 nm. TEM-foil preparation followed standard techniques commonly used for ceramic materials which involve diamond cutting, ultra-sound drilling, mechanical grinding, dimpling, Ar-ion thinning to perforation, and light carbon coating to minimize electrostatic charging under the electron beam. In addition to conventional TEM analysis, high-resolution electron microscopy (HREM) imaging was performed to study two-grain boundaries (Si_3N_4/Si_3N_4 interfaces) utilizing a JEOL JEM 4000EX (top entry) operating at 400 kV with a point resolution of 0·18 nm.†

Surface analysis of commercially available Si_3N_4 powders (direct nitridation: Denka SN-9FW, diimide precipitation: Tosoh TS-10) was performed by XPS (Perkin Elmer PHI 5600) and FT-IR spec-

*The material investigated was fabricated by Dr H. Schönfelder at the Max-Planck-Institute in Stuttgart under the assistance of Prof. R. Riedel and Prof. F. Aldinger.

†The high-resolution electron microscope is located at the Max-Planck-Institute in Stuttgart and the HREM work presented in Figs 6 and 7 was performed with the support of Prof. M. Rühle.

troscopy (Digilab FTS 15/80; reflection mode). Qualitative phase analysis from bulk materials was determined by standard powder X-ray diffraction (Seifert XRD3000P) techniques. In addition to TEM studies, quantitative microstructure analysis was performed using an image processing system (Quantimet 5000). The evaluation of the microstructure was based on CF_4 plasma-etched cross sections of the corresponding materials obtained by scanning electron microscopy (SEM) using a Jeol JSM-6400 instrument operating at 30 kV. The K_{Ic}-values of the different Si_3N_4 materials were determined by Vickers hardness indentation measurements (10 kg, 10 s, 0.5 mm/min) as well as Chevron notch experiments. In addition, crack propagation studies were performed by SEM and correlated to the grain-boundary chemistry (sintering aid composition) in these materials.

2.3 Microanalysis, EELS characterization

Electron energy-loss spectroscopy (EELS) studies were performed utilizing a PEELS spectrometer (Gatan, 666) with parallel detection, which is fitted to the Philips CM20FEG (field emission gun) microscope operating at 200 kV. Under optimized working conditions, an energy resolution of 0·75–0·80 eV was achieved, which also allows for energy-loss near edge structure (ELNES) analysis. It should be noted that during EELS measurements of the glass phase, present at triple-grain pockets as well as along interfaces, these amorphous residues can easily be damaged since a high energy field emission gun is utilized. In order to limit possible changes in the local chemistry owing to beam damage, which would exclude quantitative chemical analysis, a slightly defocused and spread beam was used during acquisition of the different spectra. These only slightly altered acquisition conditions do not influence the energy resolution of the spectrometer.

3 Results and Discussion

3.1 Characterization of starting powders

In general, there are two major routes regarding processing of ceramic components: (i) the classic way of utilizing crystalline ceramic starting powders to shape powder-compact preforms, which are subsequently densified via liquid assisted sintering and (ii) the utilization of liquid, highly viscous precursors (commonly polysilazanes), which are heat treated after initial cross-linking to form amorphous pre-ceramics that can finally be transformed into fully crystalline ceramics with a low oxygen content.[14–16] In this section, only the characterization of crystalline Si_3N_4 starting powders by TEM is presented since polymer-derived powders are typically amorphous. However, the microstructure development of such amorphous pre-ceramics during subsequent heat treatment up to 1600°C is discussed in more detail in the following section.

3.1.1 Particle-surface chemistry (organometallic doping)

Apart from the characterization of crystalline powders, which commonly focuses on the determination of intrinsic defects and the imaging of amorphous oxidized surface films, the influence of the oxygen distribution and chemical bonding state as well as the particle shape and surface chemistry (OH-group versus fluorine occupation) on both the doping via organometallic precursors and the densification rate of the powder compacts was investigated.[17–20] Two Si_3N_4 powders, processed via direct nitridation (Denka) and diimide precipitation (Tosoh), were studied. Photoelectron spectroscopy (XPS) studies revealed a lower oxygen concentration at the Si_3N_4 particle surface for the Denka powder SN-9FW compared to the Tosoh powder TS-10, (see Fig. 1(b)). In addition, a high fluorine concentration was observed in the Denka powder. The low oxygen content is closely related to the high fluorine content since the powder, processed via direct nitridation, was subsequently HF leached, which reduces the continuous silica layer on the Si_3N_4 particle surface and, furthermore, introduces fluorine into the powder and reduces the amount of surface OH-groups. Infrared spectroscopy (FT-IR) revealed an increasing height of the absorption peak of the OH-stretching vibration at 3750 cm^{-1} for the Tosoh powder in contrast to the Denka Si_3N_4 powder, as depicted in Fig. 1(a).

Comparing TEM micrographs of the two different synthesized starting powders, the data obtained by spectroscopic means are consistent with the TEM observations of the particle surfaces with high spatial resolution.[20] Moreover, densification studies performed by *in situ* dilatometry during gas-pressure sintering showed a clear difference between the two starting powders investigated. By adding sintering aids via organometallic compounds, a higher densification rate was monitored for the Tosoh powder (diimide precipitation, high OH-group occupancy). It is thought that a homogeneous coverage of the Si_3N_4 particle surface with the sintering aid in combination with a continuous SiO_2 layer leads to a higher density of contact points, where liquid can locally be formed at elevated sintering temperatures, which results in the observed enhanced densification rate. Therefore, the use of organometallic compounds is

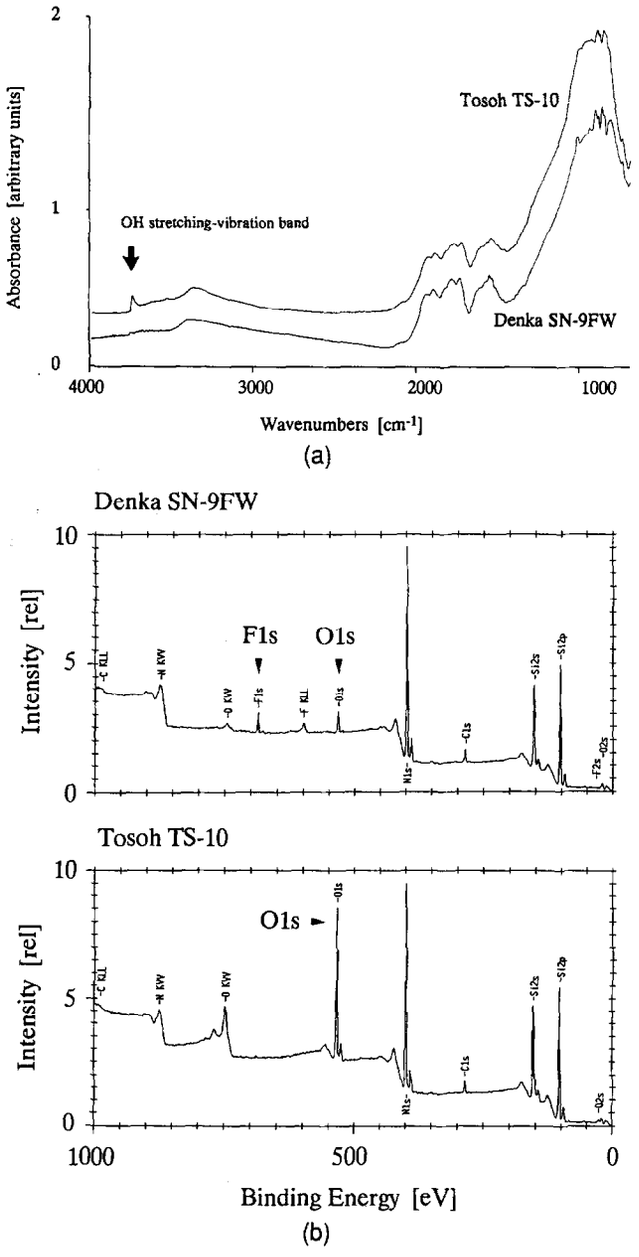

Fig. 1. (a) FT-IR spectra of the undoped Tosoh TS-10 (diimide process) and Denka SN-9FW (direct nitridation) Si_3N_4 powders. Note the higher OH-stretching vibration intensity at 3750 cm^{-1} for the Tosoh powder indicating a higher OH-group occupancy which favours doping via organometallic precursors. (b) XPS spectra for both Si_3N_4 powders showing strong variations in the surface oxygen and fluorine content.

favourable for Si_3N_4 processing, however, it should be noted that this potential advantage strongly depends on the particle-surface chemistry of the powder (oxygen content, fluorine content, OH-groups). XPS in addition to FT-IR studies clearly revealed that a high OH-group occupancy, a high surface oxygen content (not the total oxygen content), and a low fluorine concentration, as given for the Tosoh TS-10 powder, are necessary requirements in order to fully exploit the potential of chemical doping.

In contrast, Fig. 2 also reveals an inhomogeneous distribution of Y_2O_3 addition (via organometallic precursors) for the Denka Si_3N_4 powder with a relatively low OH-group occupancy and a thin amorphous oxidized layer on the particle surface. This study unequivocally showed that particle–surface chemistry strongly affects the distribution of sintering aids dispersed within the Si_3N_4-powder compact as well as the densification behaviour of the material. Moreover, it should be emphasized that a distinction between surface oxygen and bulk oxygen (partially dissolved in the crystal lattice) has to be made.

3.2 Microstructure development during densification

3.2.1 Powder derived ceramics (transient crystalline phases)

Densification behaviour of ZrO_2-fluxed SRBSN was monitored by *in situ* dilatometry and correlated to the microstructural development of the material using conventional TEM, HREM and AEM. Two distinct densification events were observed at 1730–1750°C and at 1900–1920°C. The densification rate during the first dilatometer maximum was relatively low with 0·5 μm/min compared to the second maximum which was strongly pronounced with 70 μm/min. The low densification rate of the first dilatometer event can be related to the formation of a silica-rich highly viscous liquid phase, which mainly promotes rearrangement of the matrix grains. Conventional TEM investigations of TEM-foils which corresponded to the two dilatometer maxima showed marked differences regarding both crystalline phase assemblage and microstructure development, as reported in more detail elsewhere.[21]

The low-temperature sintered body consisted of homogeneously fine-grained β-Si_3N_4 particles with a relatively high amount of residual porosity of approximately 10 vol%, as estimated by TEM. As opposed to the fully dense material, no elongated large β-Si_3N_4 grains were present at this stage of microstructural development. However, some extended aggregates of the crystalline ZrO_2 secondary phase (up to 5 μm in diameter), which are presumably due to agglomeration during powder processing, were occasionally observed. It is important to note that these agglomerates are only present under the conditions of the first dilatometer maximum and were not observed in the densified SRBSN materials. This indicates that the unstabilized zirconia addition does not (or only in a very limited amount) contribute to the liquid-phase formation process within the low-temperature densification regime.

Apart from the large agglomerates crystalline ZrO_2 secondary phases are present at three- and four-grain junctions. In addition to the ZrO_2,

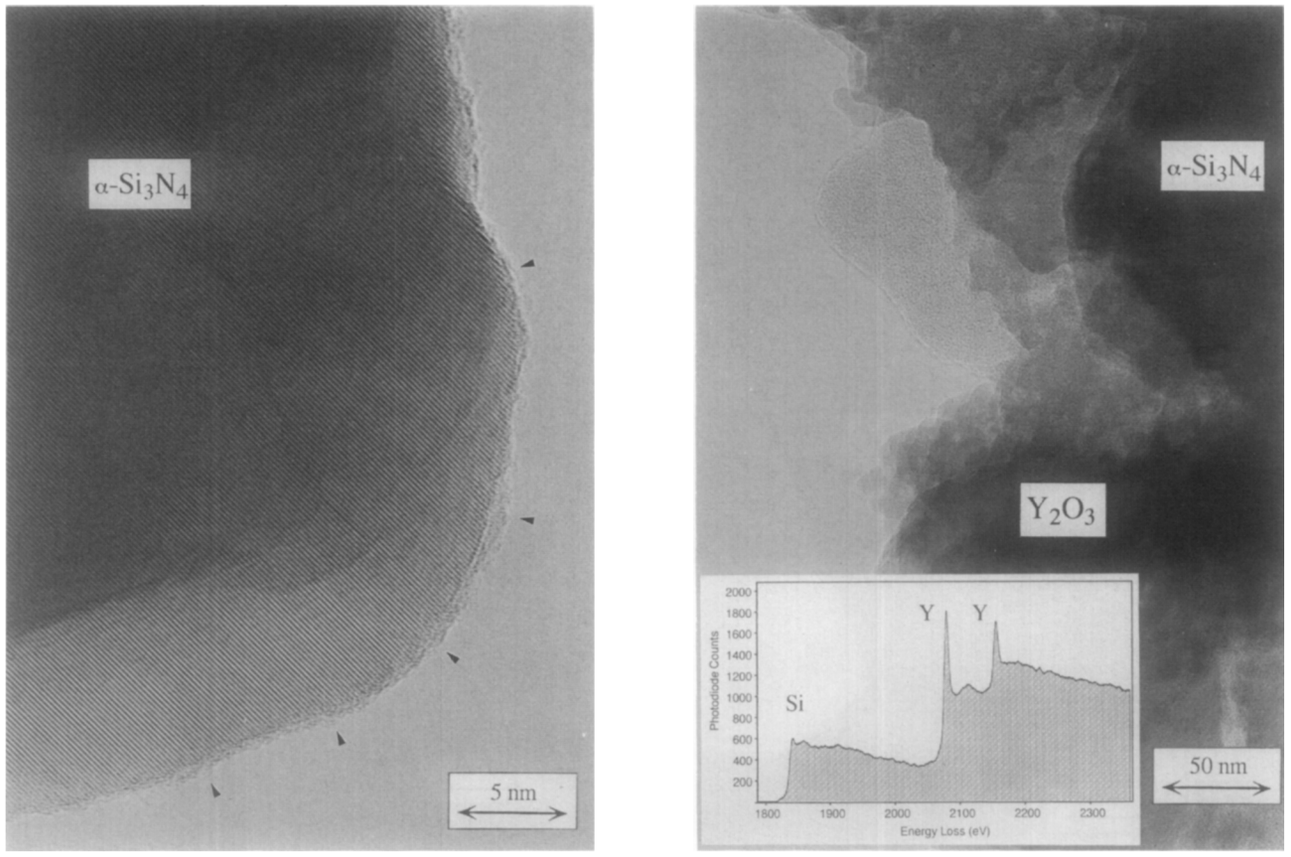

(a) (b)

Fig. 2. TEM bright field images of (a) the Tosoh TS-10 powder homogeneously covered by a thin amorphous yttria layer (organo-metallic doping) and (b) the Denka SN-9FW powder, where an inhomogeneous precipitation of amorphous yttria is shown. Note that the inhomogeneity in sintering aid distribution is based on the particle surface chemistry, i.e. the relatively low OH-group occupancy and the high fluorine content of the nitrided powder.

Si_2N_2O was also observed in the material which corresponds to the first low-temperature sintering event. Although, with respect to its thermal stability, Si_2N_2O is a transient secondary phase in the Si_3N_4–ZrO_2 system, it plays an important role during liquid phase sintering of Si_3N_4 ceramics. This becomes evident comparing the characteristic microstructural features of Si_2N_2O microcrystals from the Si_3N_4–ZrO_2 material with other liquid-phase sintered Si_3N_4-based materials, e.g. the SiO_2–Si_3N_4 binary system.[22] As shown in Fig. 3, Si_2N_2O contains numerous small spherical intragranular inclusions which were identified as α-Si_3N_4 by means of HREM, CBED and small probe microanalysis. This is in agreement with recent observations obtained from Si_2N_2O microcrystals formed during liquid-phase sintering in the system SiO_2–Si_3N_4.[23] Based on the TEM observations, the reaction scheme which is given in (2) is proposed.

$$SiO_2 + \beta\text{–}Si_3N_4 + \alpha\text{–}Si_3N_4 \Rightarrow 2\ Si_2N_2O + (\alpha\text{-}Si_3N_{4(\text{nuclei})}) \quad (2)$$

In the ZrO_2-fluxed SRBSN materials an eutectic SiO_2-rich liquid is formed at approximately 1680°C and, since the α/β Si_3N_4 phase transformation is not yet completed, Si_2N_2O is formed surrounding α-Si_3N_4 particles. It is important to note that Si_2N_2O is a transient phase in the temperature range of 1700–1800°C and will decompose at higher sintering temperatures, which influences the densification behaviour of the material. Therefore, the relatively low densification rate of the first dilatometer maximum of 5 μm/min can be related to the formation of a SiO_2-rich eutectic liquid enhancing particle rearrangement. Moreover, the results suggest that the formation of Si_2N_2O grains during the first dilatometer maximum influences further densification, because the SiO_2 content in the liquid phase present at elevated temperatures is changed. With increasing sintering temperature and duration of the experiment, the SiO_2 content and hence the amount of liquid is lowered by the Si_2N_2O formation, which strongly retards further densification.

Upon sintering, the material was fully densified and no large secondary-phase agglomerates were observed. Moreover, Si_2N_2O is no longer present in the microstructure, owing to the thermal degradation of Si_2N_2O above 1830°C[22] releasing additional SiO_2 and Si_3N_4 and, therefore, increasing the liquid-phase amount in the Si_3N_4–ZrO_2 system. Thus, both Si_2N_2O and ZrO_2 participate in the

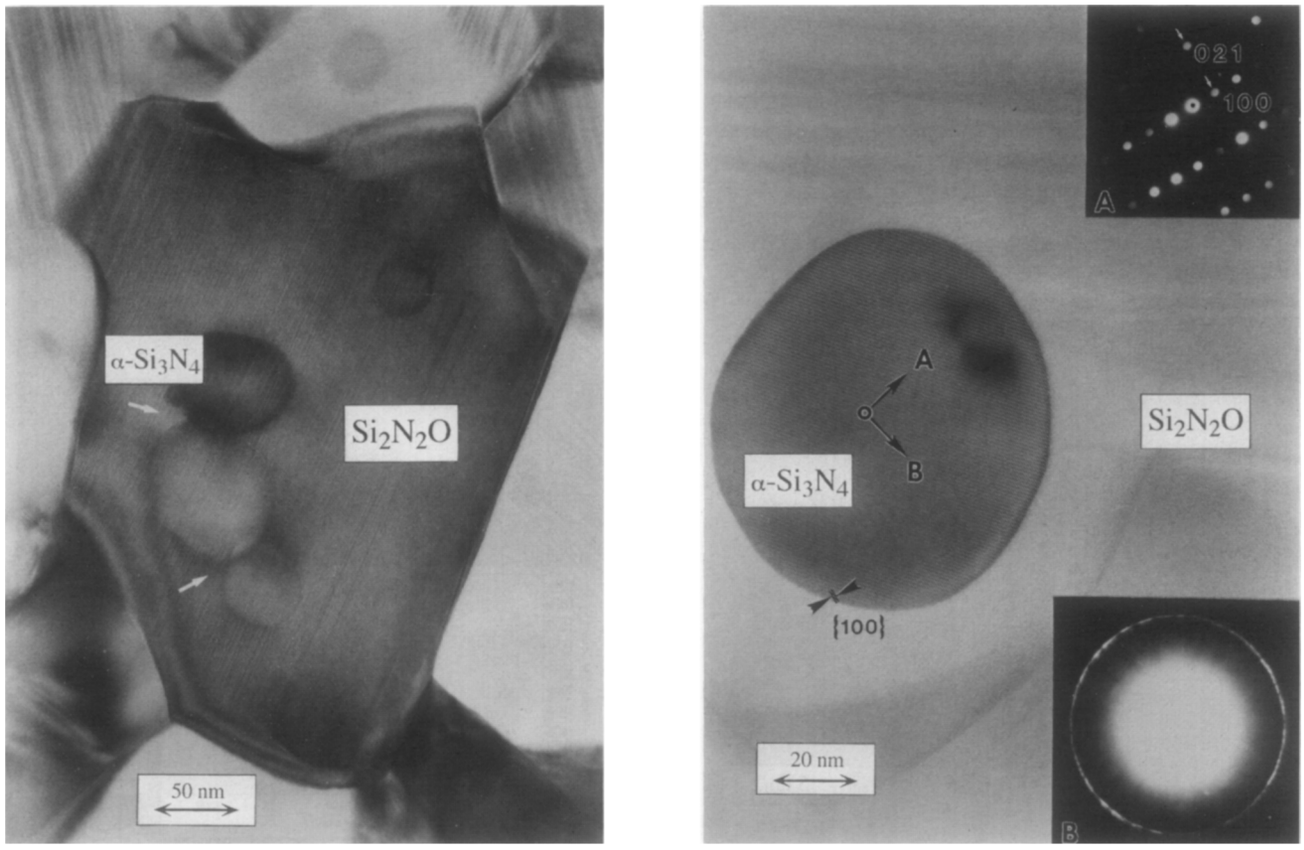

(a) (b)

Fig. 3. (a) TEM bright field image and (b) HREM micrograph of a similar area showing an Si_2N_2O crystal with intergranular spherical α-Si_3N_4 inclusions (arrowed). The image is taken from the ZrO_2-doped SRBSN microstructure equivalent to the first low-temperature dilatometer maximum. Note the high density of planar defects in the Si_2N_2O grain. At higher sintering temperatures, Si_2N_2O is no longer observed in the microstructure (transient phase).

liquid-phase formation and give rise to the strongly pronounced densification, as observed in the second dilatometer maximum. It should be noted that the microstructure development of dense ceramic materials can only be understood in light of the transient crystalline phases which form and subsequently decompose during the densification process.

3.2.2 Polymer derived ceramics (crystallization)

In the Si–C–N system, synthesis of polymer-based precursors was performed with respect to optimization of viscosity, wettability, long-term stability and maximum ceramic yield.[13,16] Improved thermal behaviour as one aim of the development of such polymer-derived ceramics was investigated in the temperature range up to 1600°C in air.[24] Heat treatment at 1400°C in N_2-atmosphere results in a nearly completely amorphous silicon carbonitride matrix phase $Si_{3+x}N_4C_{x+y}$.TEM observations revealed that, in contrast to XRD analysis, small precipitates of α-Si_3N_4, α-SiC, and graphite are already present within the amorphous matrix. The amount of these phases is, however, below the detection limit of the XRD measurement. On further oxidizing annealing above 1400°C, the amorphous material continues to crystallize. The α-Si_3N_4 crystals continuously grow, forming large microcrystals, as depicted in Fig. 4.

α-SiC continues to crystallize as well, but no-enhanced grain growth was observed. The overall SiC crystallite size is approximately 10–20 nm. Apart from Si_3N_4 (microcrystals) and SiC (nano-sized crystallites) residual graphite was also observed in the material. The presence of graphite is consistent with the chemical composition of the polysilazane precursor. It can be concluded that the phase assemblage within the material did not change during heat treatment up to 1600°C in air. The material studied underwent complete crystallization during oxidation at 1600°C for 50 h. No residual amorphous phase was observed during TEM investigations. The oxidation resistance of this covalently bonded ceramic micro-nanocomposite is related to the formation of a passivating SiO_2-surface layer. It should be noted that the composition of such materials may be changed in a relatively wide range (Si_3N_4–SiC–C) via chemical modifications. Moreover, it is thought that by changing maximum pyrolysis temperature, heating rate, holding time, and annealing atmosphere, the resulting microstructure (micro/nano) can also be markedly changed. Thus, tailoring of microstruc-

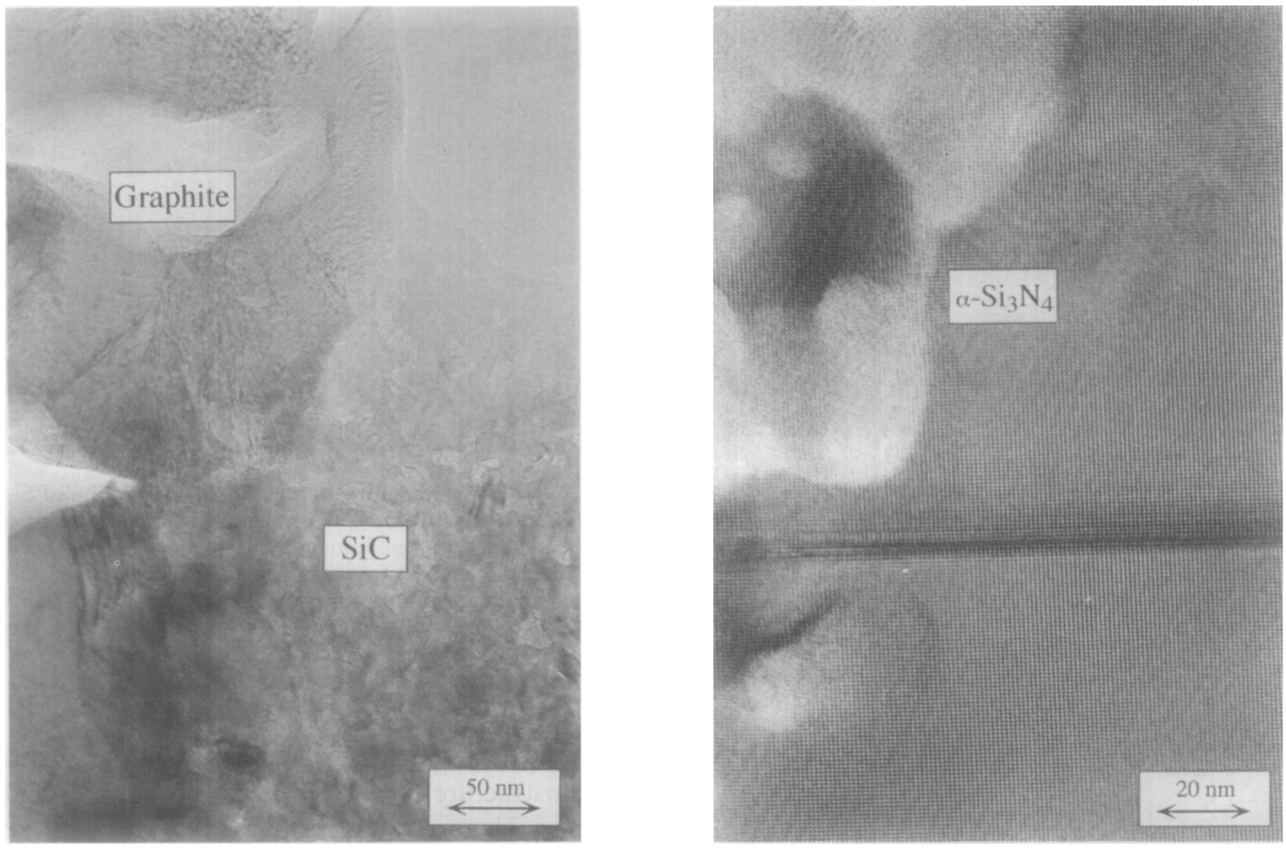

Fig. 4. (a) TEM bright field and (b) HREM image of the micro-nanocomposite formed after oxidizing annealing at 1600°C for 50 h of the amorphous silicon carbonitride matrix $Si_{3+x}N_4C_{x+y}$. Note that large α-Si_3N_4 microcrystals are formed opposite to the occurance of nanosized α-SiC crystallites. Graphite is only rarely observed. The phase assemblage is consistent with the phase diagram (starting composition).

tures becomes possible by applying specific crystallization procedures, which could be controlled by TEM observations.

3.3 Dense ceramic microstructures

3.3.1 Microstructure characterization (secondary phase crystallization)

Since silicon nitride cannot be fully densified by classical solid-state sintering mechanisms due to its high covalent bonding character (incongruent decomposition of Si_3N_4) and low self-diffusivity, the addition of sintering aids is a prerequisite to promote liquid-phase assisted sintering in order to achieve nearly complete densification.[25–27] During sintering, the metal oxides such as Y_2O_3 react with Si_3N_4+ SiO_2 forming an eutectic liquid which promotes both particle rearrangement and solution–reprecipitation processes.[28] Upon cooling, the liquid phase formed at high temperatures is present as an amorphous residue at triple-grain junctions and along grain and phase boundaries. Large amounts of sintering additives result in the well-known detrimental effects on high-temperature mechanical properties, e.g. creep behaviour and flexural strength, thus requiring a significant reduction in their volume fraction.[29,30] In most systems, the amorphous phase present at three- and four-grain junctions can be partially crystallized via subsequent heat-treatment. Another approach to improve high-temperature properties takes advantage of the refractory properties of rare-earth and transition element based oxides, which influence the viscosity of the liquid phase formed.[31,32] Therefore, a microstructural and microchemical characterization of the secondary phases formed after cooling or upon additional heat treatment is required.

The overall microstructure of Yb_2O_3-containing Si_3N_4 consisted of elongated β-Si_3N_4 grains, and triple-point pockets filled with remains of the liquid that formed during sintering. The multi-grain regions are homogeneously distributed throughout the material. Virtually all of the triple-point pockets were amorphous in the as-sintered material with 5 vol% Yb_2O_3 addition. The amorphous triple-grain regions were interconnected by thin amorphous grain-boundary films covering the Si_3N_4 particles. Figure 5 depicts a triple pocket which is filled with the amorphous secondary phase. Chemical analysis by EDS showed that the glass contained approximately an equal amount of both Yb and Si, a high level of oxygen, but no

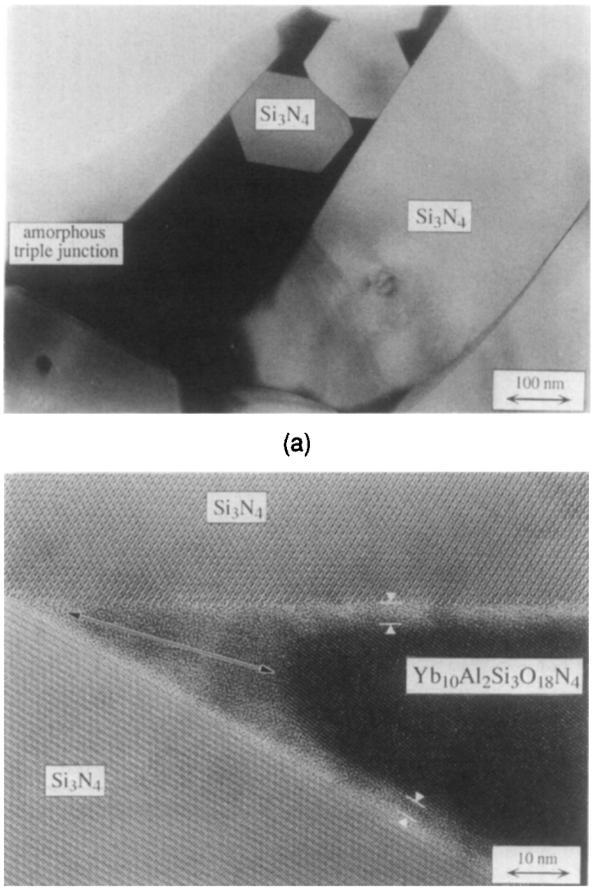

Fig. 5. TEM bright field image of (a) SSN doped with 5 vol% Yb_2O_3 after sintering and (b) SSN with 10 vol% Yb_2O_3 addition (as-sintered). In the material with the low volume fraction of sintering aid only amorphous residue is present at triple pockets while about 70% of the multi-grain junctions are already crystallized within the material containing 10 vol% Yb_2O_3 (+ 0·5 vol% Al_2O_3) forming an interconnected network of the $Yb_{10}Al_2Si_3O_{18}N_4$ phase.

nitrogen could be detected. After the heat treatment for 12 h at 1250°C, however, approximately 80% of the prior amorphous triple-grain pockets were crystalline. Both XRD and selected area diffraction (SAD) indicated that the secondary crystalline phase formed was $Yb_2Si_2O_7$. No other crystalline secondary phases were observed.

The microstructure of the material with 10 vol% Yb_2O_3 additives (which also contained about 0·5 vol% Al_2O_3 as an impurity) was substantially different compared to the material with 5 vol% Yb_2O_3 addition. After sintering, approximately 70% of the secondary phase was already crystallized in the triple junctions. $Yb_{10}Al_2Si_3O_{18}N_4$ existed as large grains extending up to several microns in size. One example of such a crystal of the interconnected secondary phase network is also shown in Fig. 5. After a post-sintering heat treatment, the secondary phase material within the triple pockets was completely crystallized. The previously large secondary-phase particles which extended over

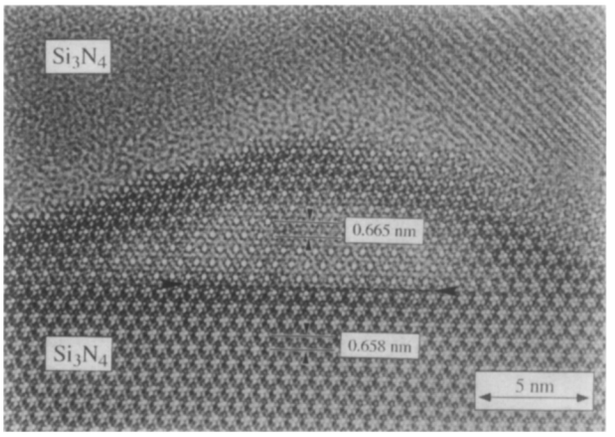

Fig. 6. HREM micrograph of an epitaxial deposition of Si_3N_4 onto a pre-existing Si_3N_4 matrix grain owing to the second phase change upon additional heat treatment. The rejection of Si and N (and Al) from the triple pockets is related to the change in composition of the secondary phase. Note that the lattice parameters of the epitaxial deposition (SiAlON phase) also change compared to the host crystal.

several triple pockets (observed in the as-sintered microstructure) were broken up into smaller grains. There was also a phase change upon heat treatment. The new secondary phase formed after heat-treating was Yb_2SiO_5 with an additional small amount of about 20% of the $Yb_2Si_2O_7$ secondary phase. The formation of these two phases is in accordance with the starting compositions in the Si_3N_4–Yb_2O_3–SiO_2 phase diagram. HREM studies along triple-grain pockets indicated an epitaxial deposition of Si_3N_4 onto pre-existing Si_3N_4 matrix grains.[33] Owing to the secondary phase change during post-sintering heat treatment, Si and N must be rejected from the triple-point pockets forming Si_3N_4 which is deposited epitaxially during the heat-treatment process. Such a deposition is shown in the HREM micrograph given in Fig. 6.

3.3.2 Fracture toughness (matrix grains versus secondary phases)

The overall microstructure in Si_3N_4 ceramics is commonly studied by scanning electron microscopy (SEM) of CF_4 plasma-etched cross sections. Quantitative microstructure analysis via image analysis allows a correlation between microstructure and bulk properties such as fracture toughness of the material. It is well established that for Si_3N_4 materials the resulting fracture resistance scales with the square root of the grain diameter, in particular, when a bimodal grain-size distribution is observed (*in situ* toughening).[34–36] However, quantitative microstructure analysis in combination with TEM analysis revealed that, in addition to the influence of the matrix grains, secondary phase crystallization can also influence fracture

toughness.[37] In case of ZrO_2 addition, the martensitic t-> m-ZrO_2 phase transformation results in the formation of local compressive stresses within the matrix. These residual stresses can cause a slight improvement in fracture resistance since the propagating crack tends to avoid such highly stressed regions. It was shown that the utilization of Sc_2O_3 as a sintering aid also resulted in an improvement in fracture resistance. Upon cooling, the material contained $Sc_2Si_2O_7$ as the only crystalline secondary phase. This phase tends to crystallize completely into the tip of the triple pockets (compare also Fig. 5(b)) and, hence, no residual glass was observed in these regions. Therefore, upon crack propagation, crack branching was often observed by SEM and TEM inspection. It is concluded that apart from matrix grain morphology and grain diameter, the crystallization of secondary phases, located at multi-grain pockets, can also affect the propagation of the crack and, therefore, influence fracture toughness. Moreover, it should be noted that grain-boundary chemistry was found to also affect fracture resistance. Depending on the interface chemistry and the resulting grain boundary bonding character, trans-granular fracture is favoured compared to the commonly observed intergranular fracture mode. Strong interface bonding, as observed for the addition of ZrO_2 + Al_2O_3 as sintering aids, leads to a marked reduction in fracture toughness since predominantly transgranular fracture occurred.[38]

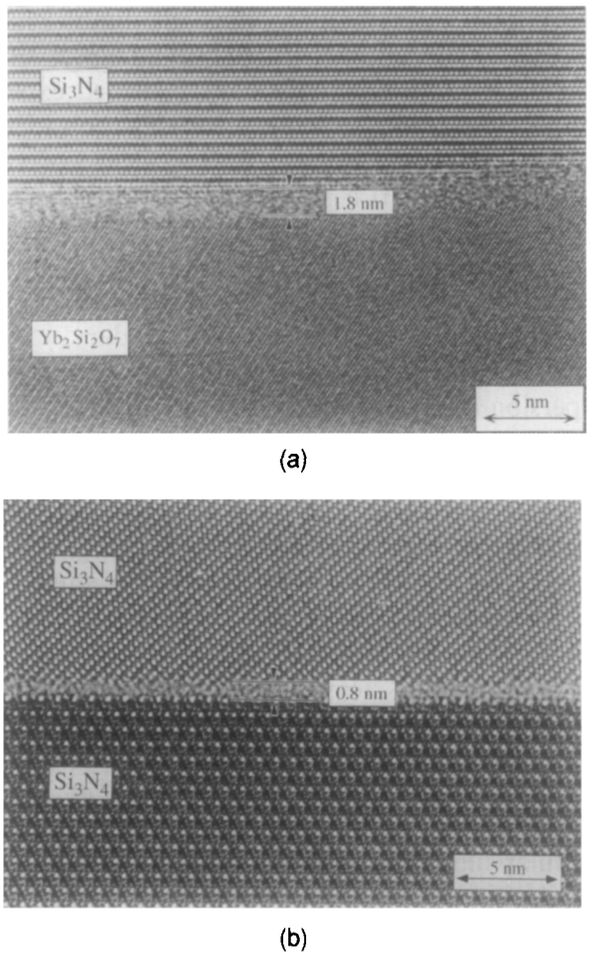

Fig. 7. HREM micrographs (400 kV) of (a) $Yb_2Si_2O_7/\beta$-Si_3N_4 phase boundary observed in the annealed SSN doped with 5 vol% Yb_2O_3 and (b) β-Si_3N_4/β-Si_3N_4 grain boundary found in a MgO-fluxed silicon nitride. Note that the intergranular film thickness along phase boundaries is typically wider compared to the width at grain boundaries.

3.3.3 Characterization of interfaces (amorphous grain-boundary films)

Apart from characterizing secondary phase crystallization, high-resolution electron microscopy (HREM) was utilized to study Si_3N_4 interfaces. Owing to the liquid phase involved during sintering at elevated temperatures, amorphous residue of this liquid is commonly present at multi-grain regions (see also Fig. 5). Moreover, Si_3N_4-grains are always separated by a continuous amorphous intergranular film with the only exception being low-energy grain boundaries.[39] Such intergranular films are present at both homophase (Si_3N_4/Si_3N_4) and heterophase (Si_3N_4/crystalline secondary phase) boundaries. The film thickness of hetero-phase boundaries was shown to always be greater than the thickness observed along homophase boundaries, as depicted in Fig. 7. The presence of such amorphous interfacial glass profoundly affects the mechanical properties of Si_3N_4-based ceramics, particularly at high service temperatures. Therefore, a control of these films is most desirable with respect to materials performance.

It is important to note that these interfacial glassy films revealed a constant thickness within each of the materials investigated. In general, different TEM techniques can be applied for the detection and evaluation of the intergranular film thickness. The measurement of the film thickness by diffuse dark-field imaging resulted in values 50–100% larger than those determined by HREM imaging. Defocus Fresnel fringe imaging is an indirect method of obtaining intergranular film width. With this method the film thickness was overestimated by about 20–35%, with the largest error stemming from the uncertainty in the exact location of the Fresnel fringe maxima. Therefore, high-resolution lattice imaging is a method capable of the resolution necessary to obtain detailed information of the boundary and the intergranular phase itself. It was shown to be applicable to quantitatively evaluate the intergranular film thickness in Si_3N_4 materials with an accuracy of $\pm$ 0·1 nm.[40–42]

Model experiments on high-purity Si_3N_4 materials with and without a low amount of CaO addition seemingly support the model first presented by Clarke[43,44] on the equilibrium thickness of

amorphous intergranular films in liquid-phase sintered Si_3N_4 ceramics. Statistical analyses of a number of grain-boundary films provided experimental verification of these theoretical considerations.[42] The model involves the influence of two repulsive forces: (i) a steric force which is caused by the steric hindrence of SiO_4 tetrahedra present in the silicate films and (ii) a force produced by an electrical double layer along the interface owing to the segregation of cations at the boundary, which is thought to balance the attractive van der Waals dispersion force that acts across the interface. This force balance results in the observed formation of an equilibrium film thickness. Si_3N_4 materials with different rare-earth and transition-element oxide additions as well as variations in volume content of sintering aids were studied. HREM studies in conjunction with analytical electron microscopy (AEM) revealed that differences in grain-boundary film thickness are related to changes in chemical composition of the intergranular films, which depends on the material analyzed, i.e. its densification aid and impurity content (see also Fig. 7).

The results clearly show a dependence of intergranular film thickness on chemical composition. No clear dependence on volume fraction of additives was found. Upon post-sintering heat treatment crystalline secondary phases form at triple-grain regions. Depending on the secondary phases formed (crystal chemistry), interface chemistry can be altered and hence grain-boundary film thickness will also be markedly changed.

3.3.4 Microanalysis (electron energy-loss spectroscopy)

In order to study, apart from cation concentration, the influence of anions at the interface on the intergranular film thickness and the resulting mechanical properties, a Si_3N_4 material was fabricated via hot-isostatic pressing without the addition of commonly used sintering aids. However, a small amount of fluorine was added to the system via powderized teflon.[45] The incorporation of fluorine into the material was deliberately chosen, in order to weaken the interfaces. Electron energy-loss spectroscopy (EELS) revealed the presence of fluorine both at the triple-grain junctions and the grain-boundary films. Through the determination of the F/O-ratio for the spectra obtained from triple pockets and interface regions, no major compositional changes were detected, which seemingly suggests a homogeneous secondary phase composition within the material. Assuming a constant grain-boundary chemistry, a constant film thickness is expected. In contrast, with respect to the incorporation of fluorine into the SiO_2-glass structure, a small increase in film thickness (δ = 0·1 nm) was also expected in comparison to the pure silica containing material (1·0 nm). This is due to the fact that the replacement of oxygen by fluorine, which have almost identical ionic radii with 140 pm and 133 pm for O^{2-} and F^-, respectively, requires two fluorine ions to allow for charge balance (compare also Fig. 8). The HREM observations are consistent with the obtained EELS results and, in addition, that the grain-boundary structure is also influenced by the anion concentration, i.e. the fluorine content at the interface. Preliminary results showed an enhanced intergranular fracture of the F-doped material compared to the undoped sample as well as a lower creep resistance.[46] This latter result is consistent with the lower HIPing temperature needed in the F-doped system to achieve full densification. The variation in mechanical response of the F-doped samples compared to the undoped materials is attributed to changes in the glass structure (glass chemistry), owing to the incorporation of fluorine.

3.4 Dynamic microstructures

In this section, the variation of ceramic microstructures, which are commonly thought to be very stable even under service conditions, is investigated after their exposition to high temperatures and high local stresses. Emphasis is placed on the structural and chemical changes in Si_3N_4 ceramics doped with m-ZrO_2 which are observed after cyclic fatigue testing of the material.[47] Before testing, a typical Si_3N_4 microstructure with m-ZrO_2 present at multi-grain pockets was observed by TEM, as depicted in Fig. 9.

Upon mechanical testing, one unexpected result which emerges from the microstructural characterization of the m-ZrO_2 doped Si_3N_4 ceramic was the formation of newly formed amorphous phase owing

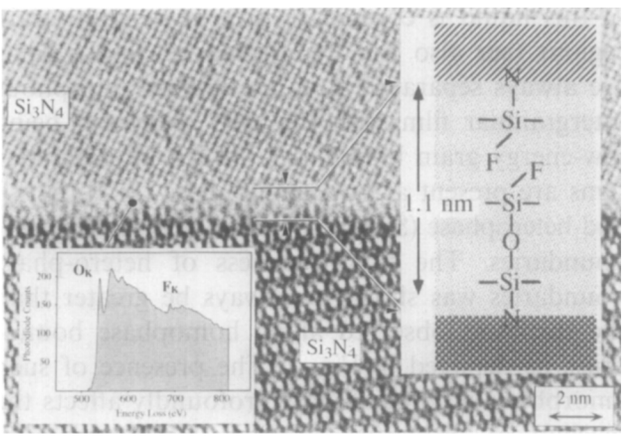

Fig. 8. HREM image (400 kV) of an intergranular film present in fluorine-doped Si_3N_4 HIPed without the addition of sintering aids. Note that F could be detected along the interface by EELS measurements (see inset). The variation of the glass structure due to the incorporation of F (replacing the bonding O) is schematically indicated in the inset on the right.

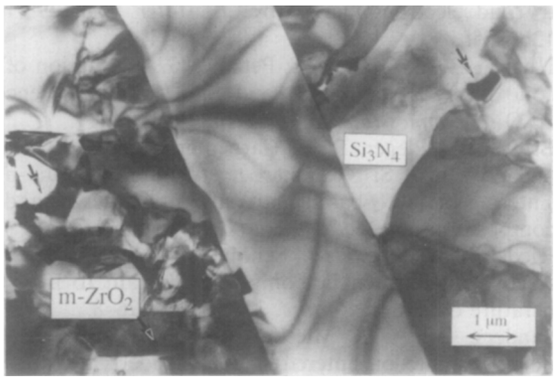

(a)

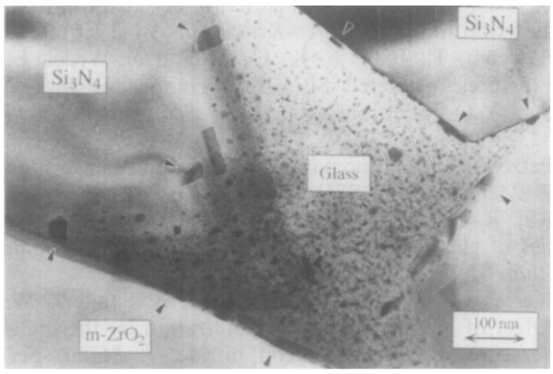

(b)

Fig. 9. TEM bright field images of ZrO_2-doped SRBSN (a) as-sintered microstructure with m-ZrO_2 homogeneously distributed at triple pockets. (b) Microstructural changes observed after cyclic fatigue at 1100°C. Note that the m-ZrO_2 dissolved in the residual glass and, upon cooling, started to reprecipitate in the glass pocket as well as along the phase boundaries (epitaxy) owing to supersaturation of the glass.

to the local dissolution of zirconia in the pre-existing glass, as shown in Fig. 9(b). This surprising observation of the partial decomposition of m-ZrO_2 at rather low testing temperatures seemingly suggests that the potential application of this 'high-temperature ceramic' is well below 1200°C. Moreover, it should be borne in mind that crystallization of residual glass pockets via post-sintering heat treatments in these materials is, in general, believed to overcome the problem of degradation of high-temperature properties. Since the replacement of amorphous triple pockets by crystalline secondary phases, e.g. the formation of m-ZrO_2 with a high thermal stability, would strongly reduce the amount of glass which softens at elevated temperatures. Therefore, high temperature properties are commonly thought to improve with secondary phase crystallization. However, the results presented clearly show that even the formation of m-ZrO_2 does not allow for a sufficient material performance above 1100°C. This is due to the formation of additional residual glass (newly formed) owing to the local dissolution of ZrO_2 under the applied temperature and stress. It is concluded that high-temperature performance of Si_3N_4-based ceramics can only be improved by post-sintering heat treatment when the formation of secondary phases can be initiated, which are stable even under the applied high temperature and high local stresses, i.e. the occurance of newly formed residual glass has to be suppressed.

4 Conclusions

The results presented were thought to underline the importance of the TEM technique for a detailed characterization of ceramic microstructures with high spatial resolution. The TEM technique can be applied, in addition to spectroscopic methods, in most of the relevant steps involved during ceramic processing such as:

- Powder processing; organometallic doping (powder surface chemistry);
- Microstructure development during densification (transient crystalline phases);
- Crystallization of polymer derived ceramics (micro/nanocomposites);
- Secondary phase crystallization (phase change upon post-sintering heat treatment);
- As-sintered microstructures (amorphous intergranular films);
- Microstructural changes under service conditions (formation of new glass).

Transmission and analytical electron microscopy is hence shown to be a very helpful characterization tool which allows us to expand our understanding of the development of ceramic microstructures. This technique can be: (i) applied in order to investigate the formation process of complex ceramic microstructures such as polymer-derived pre-ceramics and, based on the understanding of microstructure formation, (ii) used to influence materials processing. This enables the direct influence of materials fabrication with respect to tailoring ceramic microstructures for potential application requirements.

Acknowledgements

C. Kunert, University of Bayreuth, is acknowledged for her excellent preparation of the delicate TEM-foils. Dr J. Göring, German Aerospace Research Establishment (DLR), is thanked for cyclic fatigue testing of ZrO_2-doped SRBSN. We are greatly indebted to Prof. M. Rühle who strongly supported the work presented on HREM studies of interfaces in Si_3N_4 ceramics during the stay of the primary author at the Max-Planck-Institute in Stuttgart.

References

1. Reimer, L., *Transmission Electron Microscopy*, 3rd Edition, Springer-Verlag, Berlin, 1993.
2. Spence, J. C. H. & Zuo, J. M., *Electron Microdiffraction*, Plenum Press, New York, 1992.
3. Braue, W., Konvergente Elektronenbeugung in der analytischen Elektronenmikroskopie keramischer Werkstoffe – eine Anleitung für die Praxis. *Mat.-wiss. u. Werkstofftech.*, **21** (1990) 72–84.
4. Redjamimia, A. & Morniroli, J. P., Application of microdiffraction to crystal structure identification. *Ultramicroscopy*, **53** (1994) 305–17.
5. Greil, P. & Weiss, J., Evaluation of the microstructure of β-SiAlON solid solution materials containing different amounts of amorphous grain boundary phase. *J. Mater. Sci.*, **17** (1982) 1571–8.
6. van Tendeloo, G., Anders, L. & Thomas, G., Electron microscopy investigation of the ZrO_2–ZrN system. II: Tetragonal and Monoclinic ZrO_2 Precipitation. *Acta Met.*, **31** (1983) 1619–25.
7. Bonnell, D. A., Tien, T.-Y. & Rühle, M., Controlled crystallization of the amorphous phase in silicon nitride ceramics, *J. Am. Ceram. Soc.*, **70**(7) (1987) 460–5.
8. Rühle, M., Ma, L. T., Wunderlich, W. & Evans, A. G., TEM studies on phase stabilities of zirconia ceramics. *Physica B*, **150** (1988) 86–98.
9. Falk, L. K. L. & Dunlop, G. L., Crystallization of the glassy phase in an Si_3N_4 material by post-sintering heat treatments. *J. Mater. Sci.*, **22** (1987) 4369–76.
10. Cinibulk, M. K., Thomas, G. & Johnson, S. M. Grain-boundary-phase crystallization and strength of silicon nitride sintered with a YSiAlON glass. *J. Am. Ceram. Soc.*, **73**(6) (1990) 1606–12.
11. Kleebe, H.-J. & Ziegler, G., Influence of crystalline secondary phases on densification behaviour of reaction-bonded silicon nitride during post-sintering under increased nitrogen pressure. *J. Am. Ceram. Soc.*, **72**(12) (1989) 2314–17.
12. Schönfelder, H., Silicon carbonitride ceramics from polysilazane. Ph.D. Thesis, University of Stuttgart, Germany, 1992.
13. Laine, R. M., Babonneau, F., Blowhowiak, K. Y., Kennish, R. A., Rahn, J. A., Exarhos, G. J. & Waldner, K., The evolutionary process during pyrolytic transformation of poly(N-methylsilazane) from a preceramic polymer into an amorphous silicon nitride/carbon composite. *J. Am. Ceram. Soc.*, **78**(1) (1995) 137–45.
14. Mocaer, D., Pailler, R., Naslain, R., Richard, C., Pillot, J. P., Dunogues, J., Gerardin, C. & Taulelle, F., Si–C–N ceramics with a high microstructural stability elaborated from the pyrolysis of new polycarbosilazane precursors. *J. Mater. Sci.*, **28** (1993) 2615–31.
15. Riedel, R., Passing, G., Schönfelder, H. & Brook, R. J., Synthesis of dense silicon-based ceramics at low temperatures. *Nature*, **355** (1992) 714–16.
16. Hapke, J. & Ziegler, G., Synthesis and pyrolysis of liquid organometallic precursors for advanced Si-Ti–C–N composites. *Adv. Mater.*, **7** (1995) 380–4.
17. Rahaman, M. N., Boiteux, Y. & De Jonghe, L. C., Surface characterization of silicon nitride and silicon carbide powders. *Am. Ceram. Soc. Bull.*, **65**(8) (1986) 1171–6.
18. Wang, C. M. & Riley, F. L., Alumina-coating of silicon nitride powder. *J. Europ. Ceram. Soc.*, **10** (1992) 83–93.
19. Joshi, P. N. & McCauley, R. A., Metal-organic surfactants as sintering aids for silicon nitride in an aqueous medium. *J. Am. Ceram. Soc.*, **77**(11) (1994) 2926–34.
20. Schmidt, H., Nabert, G., Ziegler, G. & Gorezki, H., Characterization and surface chemistry of uncoated and coated silicon nitride powders. *J. Europ. Ceram. Soc.*, **15** (1995) 667–74.
21. Kleebe, H.-J., Braue, W. & Luxem, W., Densification of SRBSN with unstabilized zirconia by means of dilatometry and electron microscopy. *J. Mater. Sci.*, **29** (1994) 1265–75.
22. Huang, Z. K., Greil, P. & Petzow, G., Formation of siliconoxinitride from Si_3N_4 and SiO_2 in the presence of Al_2O_3. *Ceramics International*, **10** (1984) 14–17.
23. Braue, W., Pleger, R. & Carpenter, R. W., Nucleation and growth of Si_2N_2O microcrystals during liquid-phase sintering of Si_3N_4-based materials with different additive compositions. *J. Mater. Res.*, (1995) in press.
24. Riedel, R., Kleebe, H.-J., Schönfelder, H. & Aldinger, F., A covalent micro/nano-composite resistant to high temperature oxidation. *Nature*, **374** (1995) 526–8.
25. Sanders, W. A. & Mieskowski, D. M., Strength and microstructure of sintered silicon nitride with rare-earth oxide additions. *Am. Ceram. Soc. Bull.*, **64** (1985) 304–9.
26. Tani, E., Nishijima, M., Ichinose, H., Kishi, K. & Umebayashi, S., Gas-pressure sintering of silicon nitride with an oxide addition. *Yogyo-Kyokai-Shi*, **94** (1986) 300–5.
27. Ekström, T., Falk, L. K. L. & Knutson-Wedel, E. M., Pressureless-sintered Si_3N_4-ZrO_2-composites with Al_2O_3 and Y_2O_3 additions. *J. Mater Sci. Letters*, **9** (1990) 823–6.
28. Petzow, G. & Huppmann, W. J., Liquid phase sintering. *Z. Metallkd.*, **67** (1976) 579–90.
29. Raj, R. & Lange, F. F., Crystallization of small quantities of glass (or a liquid) segregated in grain boundaries. *Acta. Met.*, **29** (1981) 1993–2000.
30. Pierce, L. A., Mieskowski, D. M. & Sanders, W. A., Effect of grain-boundary crystallization on the high-temperature strength of silicon nitride. *J. Mater. Sci.*, **21** (1986) 1345–8.
31. Cinibulk, M. K., Thomas, G. & Johnson, S. M., Strength and creep behaviour of rare-earth disilicate-silicon nitride ceramics. *J. Am. Ceram. Soc.*, **75**(8) (1992) 2050–5.
32. Lee, W. E. & Hilmas, G. E., Microstructural Changes in β-silicon nitride grains upon crystallizing the grain-boundary glass. *J. Am. Ceram. Soc.*, **72**(10) (1989) 1931–7.
33. Vetrano, J. S., Kleebe, H.-J., Hampp, E., Hoffmann, M. S. & Rühle, M., Epitaxial deposition of silicon nitride during post-sintering heat treatment. *J. Mater. Sci. Letters*, **11** (1992) 1249–52.
34. Tani, E., Umebayashi, S., Kishi, K., Kobayashi, K. & Nishijima, M., Gas-pressure sintering of Si_3N_4 with concurrent addition of Al_2O_3 and 5 wt% rare earth oxide: high fracture toughness Si_3N_4 with fiber-like structure. *Am. Ceram. Soc. Bull.*, **65**(9) (1986) 1311–15.
35. Mitomo, M. & Uenosono, S., Gas-pressure sintering of β-silicon nitride. *J. Mater. Sci.*, **26**, (1991) 3940–4.
36. Padture, N. P., *In situ* toughened silicon carbide. *J. Am. Ceram. Soc.*, **77**(2) (1994) 519–23.
37. Unger, S., Influence of microstructure development on fracture toughness in silicon nitride. Thesis, University of Bayreuth, Germany, 1994.
38. Kleebe, H.-J., Meißner, E. & Ziegler, G., Influence of Si_3N_4 interface chemistry on both grain morphology and fracture toughness, *J. de Physique IV*, **3** (1993) 1393–7.
39. Schmid, H. & Rühle, M., Structure of special grain boundaries in SiAlON ceramics. *J. Mater. Sci.*, **19** (1984) 615–28.
40. Kleebe, H.-J., Hoffmann, M. J. & Rühle, M., Influence of secondary phase chemistry on grain-boundary film thickness in silicon nitride. *Z. Metallkd.*, **83**(8) (1992) 610–17.
41. Cinibulk, M. K., Kleebe, H.-J. & Rühle, M. Quantitative comparison of TEM techniques for determining amorphous intergranular film thickness. *J. Am. Ceram. Soc.*, **76**(2) (1993) 426–32.
42. Kleebe, H.-J., Cinibulk, M. K. & Rühle, M., Statistical analysis of the intergranular film thickness in silicon nitride ceramics. *J. Am. Ceram. Soc.*, **76**(8) (1993) 1969–77.
43. Clarke, D. R., On the equilibrium thickness of intergranular glass phases in ceramic materials. *J. Am. Ceram. Soc.*, **70**(1) (1987) 15–22.

44. Clarke, D. R., Shaw, T. M., Philipse, A. P. & Horn, R. G., Possible electrical double layer contribution to the equilibrium thickness of intergranular glass phases in polycrystalline ceramics. *J. Am. Ceram. Soc.*, **76**(5) (1993) 1201–4.
45. Kleebe, H.-J., Pezzotti, G. & Nishida, T., Transmission electron microscopy characterization of a fluorine-doped Si_3N_4. *J. Mater. Sci. Letters*, (1995) in press.
46. Pezzotti, G., Matsuchita, K., Kleebe, H.-J., Okamoto, Y. & Nishida, T., Viscous behaviour of grain and phase boundaries in fluorine doped Si_3N_4–SiC composites. *Acta Metall.*, (1995), in press.
47. Göring, J., Braue, W. & Kleebe, H.-J., Microstructural response of ZrO_2-doped Si_3N_4 during static loading. In *Silicon Nitride-Based Ceramics*, Stuttgart, 4–6 October, 1993, eds M. J. Hoffmann, P. F. Becher & G. Petzow, Trans Tech Publications, Switzerland, Key Engineering Materials, **89–91**, 1994, pp. 641–6.